RSC Advances

PAPER

View Article Online
View Journal | View Issue

Cite this: *RSC Adv.*, 2021, **11**, 37824

Effect of methylene chain length of perovskite-type layered $[NH_3(CH_2)_nNH_3]ZnCl_4$ (n = 2, 3, and 4) crystals on thermodynamic properties, structural geometry, and molecular dynamics†

Ae Ran Lim *[ab]

The structure of organic–inorganic perovskite $[NH_3(CH_2)_4NH_3]ZnCl_4$ was determined; the lattice constants with monoclinic structure were determined to be a = 7.2527 Å, b = 8.1101 Å, c = 10.3842 Å, and β = 80.3436°. The crystal was almost thermally stable up to approximately 560 K. The endothermic peaks at 481 K and 506 K were assigned to the phase transition of the material. In addition, the structural characteristics and molecular dynamics of the cation were studied *via* magic angle spinning nuclear magnetic resonance experiments. Based on the results, the effects of the length of the CH_2 group in the cation of the $[NH_3(CH_2)_nNH_3]ZnCl_4$ (n = 2, 3, and 4) crystals were considered. Regardless of whether n was even or odd, the differences in the thermal and physical properties were minimal. Moreover, a difference in molecular motion relative to the length of the cation was observed only at high temperatures. These results provide useful information about the thermal stability and molecular dynamics of $[NH_3(CH_2)_nNH_3]ZnCl_4$ crystals and are expected to facilitate potential applications of such compounds in supercapacitors, batteries, and fuel cells.

Received 16th October 2021
Accepted 16th November 2021

DOI: 10.1039/d1ra07656f

rsc.li/rsc-advances

1. Introduction

Organic–inorganic hybrid compounds with perovskite structures have been extensively investigated in recent years.[1] An interesting class of compounds with perovskite structures is the diammonium series, which forms layered perovskite halogen salts, as well as the monoammonium series, which has the formula $[C_nH_{2n+1}NH_3]_2MX_4$ (n = 2, 3, …; M = Mn, Co, Cu, Zn, Cd, X = Cl, Br).[2–14] The diammonium series $[NH_3(CH_2)_nNH_3]MX_4$ has been studied because of its H-bonds and excellent stability.[11–16] $[NH_3(CH_2)_nNH_3]MX_4$ compounds with zero- and two-dimensional hybrid perovskite structures have attracted considerable attention in recent years. For M = Mn, Cu, and Cd, the structure consists of a corner-shared octahedron $(MX_6)^{2-}$ positioned between the organic layers and is two-dimensional. For M = Co and Zn, isolated tetrahedral structures form inorganic $(MX_4)^{2-}$ layers between layers of organic cations and are zero-dimensional.[17–22] $[NH_3(CH_2)_nNH_3]ZnCl_4$ (M = Zn and X = Cl) compounds crystallize in a perovskite-like structure, in which the link between adjacent $ZnCl_4$ octahedral planes is formed by the alkylene chains with NH_3 groups at both ends. The $[NH_3(CH_2)_nNH_3]$ organic chains extend along the longest c-axis, are located between the inorganic layers, and are connected to these layers through N–H···Cl hydrogen bonding.[23,24] Hence, the distance between two neighboring inorganic layers depends on the length of the organic chain. The Zn atom is surrounded by four Cl atoms to form the $ZnCl_4$ tetrahedra. These compounds are of considerable interest because of the diversity of their crystal structures, which govern their thermodynamic properties and structural dynamics. Materials such as perovskites are expected to be used for a variety of applications, including photovoltaics, photocatalysis, batteries,[25] energy storage, and micro-and nanoelectronics.[26,27] The $[NH_3(CH_2)_nNH_3]ZnCl_4$ studied here is expected to be used in various applications as it can improve relatively weak thermal stability and eco-friendly.

The synthesis and characterization of $[NH_3(CH_2)_nNH_3]ZnCl_4$ crystals with n = 2 and 3 have been reported based on X-ray diffraction.[23,24] Recently, the physicochemical properties and structural dynamics of crystals with n = 2 and 3 were investigated in terms of the changes in chemical shifts and nuclear magnetic resonance (NMR) spin–lattice relaxation times with temperature.[28,29] Although these compounds have several applications, the physical properties of $[NH_3(CH_2)_4NH_3]ZnCl_4$ crystals have not been discussed in detail.

Physicochemical properties are essential for understanding the structural dynamics of the $[NH_3(CH_2)_4NH_3]$ cation in the $[NH_3(CH_2)_4NH_3]ZnCl_4$ crystal. Solid state NMR has proven

[a]Department of Carbon Convergence Engineering, Jeonju University, Jeonju 55069, Korea

[b]Department of Science Education, Jeonju University, Jeonju 55069, Korea. E-mail: aeranlim@hanmail.net; arlim@jj.ac.kr

† Electronic supplementary information (ESI) available. See DOI: 10.1039/d1ra07656f

a useful method for study of local structure and mobility.[30] By studying the spin–lattice relaxation time $T_{1\rho}$ of the each nuclei in different environments, it is possible to obtain information about the dynamical processes occurring in different parts.

The aim of this study was to investigate the thermodynamic properties and molecular dynamics of 1,4-butanediyldiammonium tetrachlorozincate ($[NH_3(CH_2)_4NH_3]ZnCl_4$) crystals with $n = 4$. The crystal structures, phase-transition temperatures, and thermodynamic properties of the crystals were investigated using X-ray diffraction, thermogravimetric analysis (TGA), and differential thermal analysis (DTA). In addition, the chemical shifts and spin–lattice relaxation time $T_{1\rho}$ were analyzed using ^{1}H magic angle spinning (MAS) NMR, ^{13}C MAS NMR, and static ^{14}N NMR, according to the temperature change, to determine the characteristics of the $[NH_3(CH_2)_4NH_3]$ cation. The effects of the length of the CH_2 group in the cation of the $[NH_3(CH_2)_4NH_3]ZnCl_4$ crystal were considered, along with previously reported effects in $[NH_3(CH_2)_2NH_3]ZnCl_4$ and $[NH_3(CH_2)_3NH_3]ZnCl_4$. The results provide insights into the structural dynamics of $[NH_3(CH_2)_nNH_3]ZnCl_4$ crystals ($n = 2$, 3, and 4) based on the methylene chain length and are expected to facilitate potential applications in the future.

2. Experimental method

An aqueous solution containing $NH_2(CH_2)_4NH_2 \cdot 2HCl$ and $ZnCl_2$ was slowly evaporated at a constant temperature of 300 K to produce single crystals of $[NH_3(CH_2)_4NH_3]ZnCl_4$. The transparent crystals were produced within 3–4 weeks and exhibited some good quality shapes. The structure of the crystal at 298 K was analyzed using single-crystal X-ray diffraction at the Seoul Western Center of the Korea Basic Science Institute (KBSI). The crystals were mounted on a Bruker D8 Venture equipped with a 1 μs micro-focus sealed tube with Mo-Kα radiation and a PHOTON III M14 detector.

TGA and DTA experiments were performed on a thermogravimetric analyzer (TA Instrument) at a heating rate of 10 K min^{-1} between from 300 to 873 K under N_2 gas. In addition, optical observations were performed using an optical polarizing microscope in the temperature range of 300–680 K, with a Linkam THM-600 heating stage.

NMR spectra of $[NH_3(CH_2)_4NH_3]ZnCl_4$ crystals were obtained using a Bruker 400 MHz Avance II + solid-state NMR spectrometer at the Seoul Western Center, KBSI. The Larmor frequencies for the ^{1}H MAS NMR and ^{13}C MAS NMR experiments were 400.13 and 100.61 MHz, respectively. The MAS rate to minimize the spinning sideband was 10 kHz, and tetramethylsilane (TMS) was used as the standard for NMR chemical shifts. The $T_{1\rho}$ values were obtained using a $90^\circ - \tau$ pulse followed by a spin-lock pulse with a duration of τ; the width of the 90° pulse for ^{1}H and ^{13}C was 3.5–3.9 μs. In addition, static ^{14}N NMR spectra were measured under a Larmor frequency of 28.90 MHz. The ^{14}N NMR experiments were performed using one pulse with a 90° pulse width of 6 μs. The chemical shift measurements were referenced using NH_4NO_3 as the standard sample. The temperature was changed by adjusting the heater current and nitrogen gas flow, and it was maintained within ±0.5 K.

3. Results and discussion

3.1 Crystal structure

The X-ray powder diffraction pattern of the $[NH_3(CH_2)_4NH_3]ZnCl_4$ is presented in ESI 1.† Single-crystal X-ray diffraction experiments were conducted on $[NH_3(CH_2)_4NH_3]ZnCl_4$ at 298 K, and the structure was determined to be triclinic with the $P1$ space group. The lattice constants were determined to be $a = 7.2839 \pm 0.0001$ Å, $b = 8.1354 \pm 0.0001$ Å, $c = 10.4592 \pm 0.0002$ Å, and $\alpha = 77.6527 \pm 0.0005^\circ$, $\beta = 80.3358 \pm 0.0004^\circ$, $\gamma = 82.8355 \pm 0.0005^\circ$ (ESI 2†). In addition, the structures, lattice constants, and space groups of $[NH_3(CH_2)_nNH_3]ZnCl_4$ ($n = 2$, 3, and 4) were shown in ESI 3.† Among the three single crystals, the previously reported crystal structure for $[NH_3(CH_2)_3NH_3]ZnCl_4$ with $n = 3$ is shown in Fig. 1 (CCDC number: 1227730).[23]

3.2 Thermal properties

The TGA and DTA experiments were conducted at a heating rate of 10 K min^{-1}; the results shown in Fig. 2. The TGA curve shows that the crystal is almost stable up to approximately 560 K. The endothermic peaks at 481 K ($=T_{C1}$) and 506 K ($=T_{C2}$) on the DTA curve were assigned to the phase transition of the material. The molecular weight loss near 560 K marks the onset of partial thermal decomposition (T_d). $[NH_3(CH_2)_4NH_3]ZnCl_4$ undergoes a loss in molecular weight with increasing temperature. The amount remaining as solid residue was calculated from the molecular weights. Additionally, weight losses of 12% and 25% occurred at temperatures of 604 K and 622 K, respectively, due to the loss of the HCl and 2HCl moieties. Near 900 K, 95% of the total weight of the crystal was lost. To understand the TGA results, the change in the appearance of the crystals with the increase in temperature was confirmed based on optical polarizing microscopy. Even when the temperature rises from 300 K to 490 K, the single crystal is transparent and colorless, but when the temperature reaches 520 K, it starts to melt slightly, and a considerable amount of it melts at 543 K (Fig. 3).

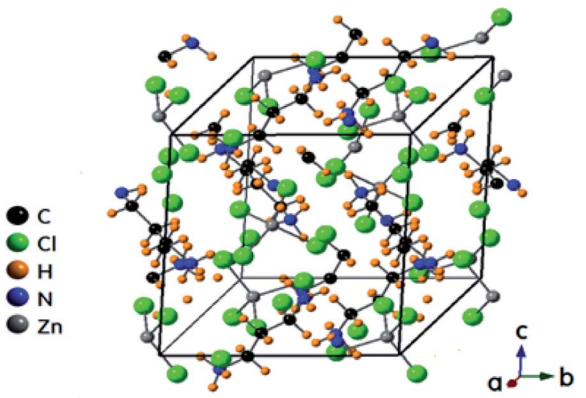

Fig. 1 Structure of $[NH_3(CH_2)_3NH_3]ZnCl_4$ crystal at 300 K (CCDC number: 1227730).

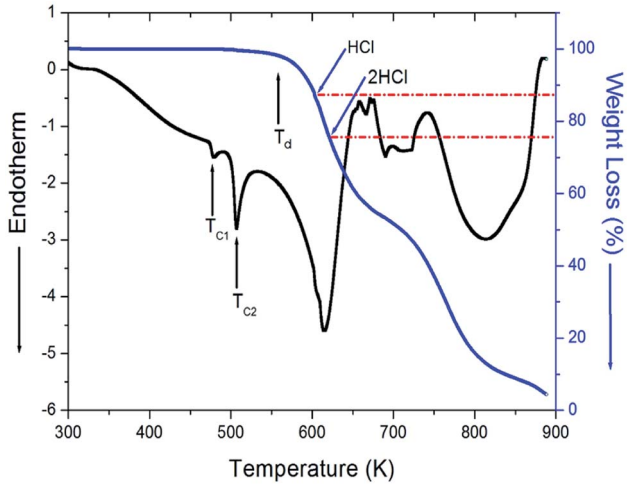

Fig. 2 Thermogravimetric analysis (TGA) and differential thermal analysis (DTA) curves of $[NH_3(CH_2)_4NH_3]ZnCl_4$.

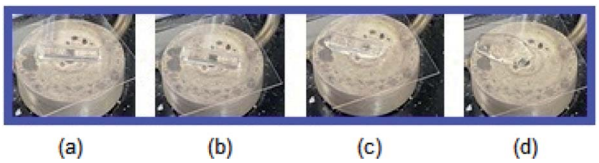

Fig. 3 Changes in crystal by optical polarizing microscopy at (a) 300 K, (b) 490 K, (c) 520 K, and (d) 543 K for $[NH_3(CH_2)_4NH_3]ZnCl_4$.

3.3 The ^{1}H MAS NMR

The ^{1}H MAS NMR spectra of the $[NH_3(CH_2)_4NH_3]ZnCl_4$ crystals were recorded according to the temperature change, and the results of the ^{1}H chemical shifts are shown in Fig. 4; the spinning sidebands are marked with pluses. The ^{1}H chemical shift at 300 K was recorded at 6.95 ppm. Below 380 K, only one resonance line is observed, but the NMR spectrum has an asymmetric shape; the left (a) and right (b) sides at the full-width-at-half-maximum (FWHM) are not equal. The asymmetric shape of the resonance line corresponds to the overlapping lines of ^{1}H in NH_3 and CH_2. The ^{1}H NMR chemical shifts were observed to be temperature-independent, which implies that the environment around ^{1}H does not change with temperature. However, above 380 K, the ^{1}H signal was split into four sharp lines (2, 3, 4, and 5), matching the number of ^{1}H signals in different environments. The number 1 denotes ^{1}H in NH_3, and the remaining four signals represent ^{1}H in CH_2, arbitrarily indicated by the numbers 2, 3, 4 and 5. The temperature-sensitive above 380 K, indicating that the structure of the environment surrounding ^{1}H in the $[NH_3(CH_2)_4NH_3]$ cation changes.

The ^{1}H MAS NMR spectra were measured with several delay times at each given temperature. The plot of spectral intensities against the delay times is described by a single exponential function. The decay rate of the proton magnetization is characterized by the spin–lattice relaxation time $T_{1\rho}$:[30,31]

$$P(\tau)/P(0) = \exp(-\tau/T_{1\rho}), \quad (1)$$

Here, $P(\tau)$ and $P(0)$ are the signal intensities at times τ and $\tau = 0$, respectively. The $T_{1\rho}$ is an important experimental quantify for the study of the local dynamics. From the slope of the logarithm of intensity–delay time plots, the ^{1}H $T_{1\rho}$ values were determined at several temperatures. An example of magnetization decay at 300 K is represented by the intensity of the signal against the delay time from 0.2 to 150 ms, as shown in Fig. 5. The intensities indicated by arrow *vs.* delay time are described by a single exponential function from the slope of their recovery traces. Moreover, the ^{1}H $T_{1\rho}$ values in $[NH_3(CH_2)_4NH_3]ZnCl_4$ were obtained as a function of inverse temperature, as shown in Fig. 6. As the temperature rises, $T_{1\rho}$ gradually increases without anomalous changes till 350 K, after which it decreases slightly. The E_a values were calculated from $T_{1\rho}\alpha \exp(\pm E_a/k_BT)$, where E_a is the activation energy for molecular motion, k_B is the

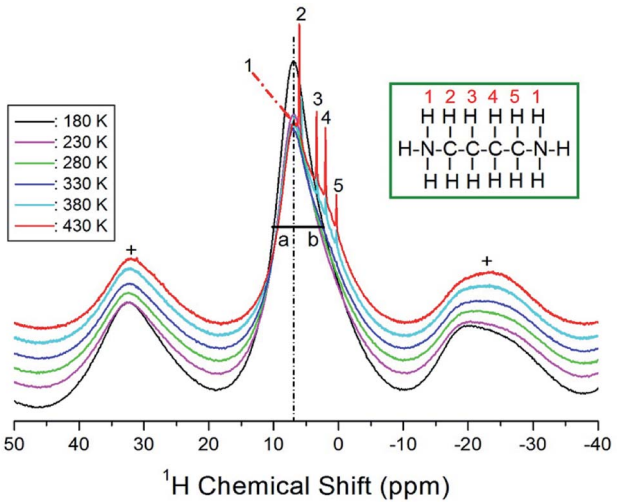

Fig. 4 MAS ^{1}H NMR chemical shifts of $[NH_3(CH_2)_4NH_3]ZnCl_4$ as a function of temperature.

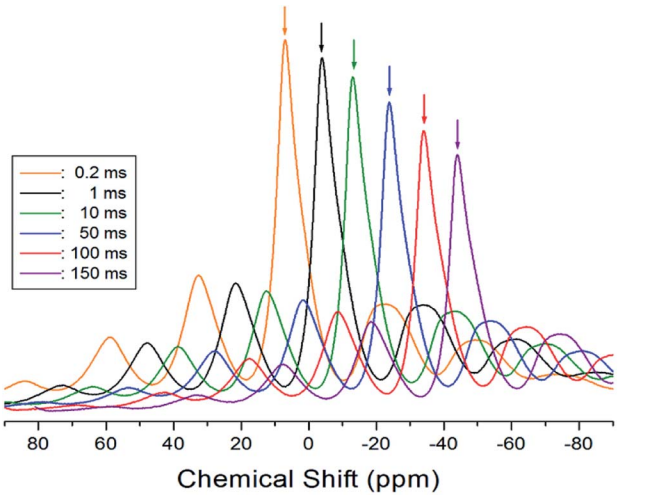

Fig. 5 Magnetization recovery curves of the MAS ^{1}H NMR spectrum in $[NH_3(CH_2)_4NH_3]ZnCl_4$ at 300 K, for delay times of 0.2–160 ms.

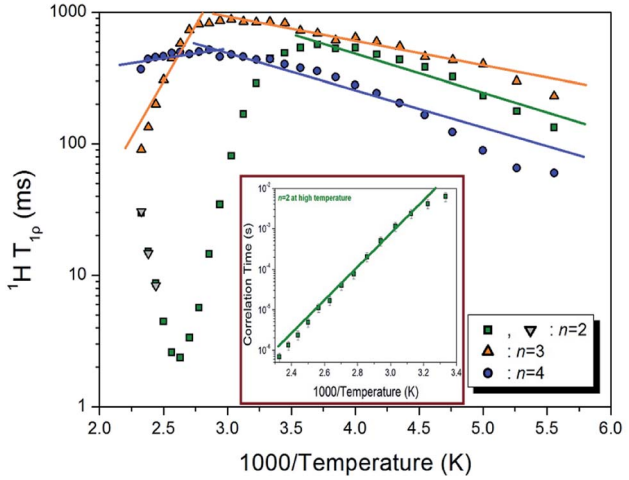

Fig. 6 ^{1}H NMR spin–lattice relaxation times $T_{1\rho}$ of $[NH_3(CH_2)_nNH_3]ZnCl_4$ (n = 2, 3, and 4) as a function of inverse temperature. The solid lines represent activation energy (inset: correlation times for $T_{1\rho}$ as a function of inverse temperature for n = 2).

Boltzmann constant, and T is the temperature. And, E_a values were determined to be 5.56 ± 0.43 kJ mol^{-1} at low temperatures and 2.30 ± 0.94 kJ mol^{-1} at high temperatures, as indicated by the solid lines in Fig. 6.

To understand the effect of the methylene chain length, we compared our results with previously reported findings regarding $[NH_3(CH_2)_2NH_3]ZnCl_4$ and $[NH_3(CH_2)_3NH_3]ZnCl_4$ (with n = 2 and 3).[28,29] The ^{1}H $T_{1\rho}$ results for the three compounds (n = 2, 3, and 4) are shown in Fig. 6 as a function of the inverse temperature. In the case of n = 2, as the temperature rises, $T_{1\rho}$ gradually increases and then reaches a maximum value of 570 ms at 270 K, before rapidly decreasing above 300 K. As shown in Fig. 6, $T_{1\rho}$ subsequently reaches its minimum value near 380 K and then tends to increase again.[28] This trend between 300 and 430 K indicates the existence of molecular motion. The $T_{1\rho}$ values are related to the correlation time τ_C for molecular motion, as per the Bloembergen–Purcell–Pound (BPP) theory,[32] which states that the local field fluctuation is caused by thermal motion. The τ_C–1000/T plot, represented by the olive line on a logarithmic scale, is shown in the inset of Fig. 6. The E_a values for ^{1}H below and above 300 K were estimated to be 4.91 ± 0.62 and 78.17 ± 4.39 kJ mol^{-1}, respectively. On the other hand, for n = 3, $T_{1\rho}$ initially increased and then abruptly decreased when the temperature increased. The $T_{1\rho}$ values of the protons were 100–1000 ms, and these values decreased abruptly at 360 K. The values of E_a for ^{1}H at low and high temperatures were 3.53 ± 0.02 and 31.86 ± 3.82 kJ mol^{-1}, respectively.[29]

The E_a values at low and high temperatures for the three compounds are listed in Table 1. At low temperatures, E_a was almost the same as the length of CH_2 in the cation, whereas at high temperatures, E_a tended to decrease.

Table 1 Activation energies E_a determined from spin–lattice relaxation times $T_{1\rho}$ in $[NH_3(CH_2)_nNH_3]ZnCl_4$ (n = 2, 3, and 4)

	^{1}H E_a (kJ mol^{-1})		^{13}C E_a (kJ mol^{-1})	
	Low temp.	High temp.	Low temp.	High temp.
n = 2	4.91 ± 0.62	78.17 ± 4.39	2.23 ± 0.45	38.88 ± 7.33
n = 3	3.53 ± 0.02	31.86 ± 3.82	1.57 ± 0.21	1.57 ± 0.21
n = 4	5.56 ± 0.43	2.30 ± 0.94	0.72 ± 0.29	6.11 ± 0.58

3.4 The ^{13}C MAS NMR

The ^{13}C MAS NMR chemical shifts for CH_2 in the $[NH_3(CH_2)_4NH_3]ZnCl_4$ crystal were recorded at several temperatures. One of the MAS ^{13}C NMR spectra at 300 K is displayed in Fig. 7, which shows that CH_2-a in the $[NH_3(CH_2)_4NH_3]$ cation is far from NH_3 and that CH_2-b is located near NH_3. The signal for the TMS reference was measured at 38.3 ppm, and this value was set to 0 ppm for the ^{13}C chemical shift. The ^{13}C NMR chemical shifts of CH_2 were separated into two inequivalent lines for CH_2-a and CH_2-b in $[NH_3(CH_2)_4NH_3]ZnCl_4$. The CH_2-a and CH_2-b resonance lines themselves were also split into two signals each. This is because the environments of the four carbons in the cation are slightly different. ^{13}C chemical shifts were observed at 24.88 and 26.26 ppm for CH_2-a and at 40.70 and 41.24 ppm for CH_2-b. In addition, the ^{13}C NMR chemical shifts were nearly temperature-independent (ESI 4†).

The ^{13}C $T_{1\rho}$ relaxations are not affected by spin diffusion, due to the small dipolar coupling, which arises because of the low natural abundance of ^{13}C. The intensity changes of the ^{13}C NMR spectrum for various delay times in $[NH_3(CH_2)_4NH_3]ZnCl_4$ were measured, and all the decay curves for CH_2-a and CH_2-b were plotted using a single exponential function. The ^{13}C $T_{1\rho}$ values shown in Fig. 8 were obtained from the slope of the recovery traces for CH_2-a and CH_2-b, in order to understand the differences in dynamics of ^{13}C at different sites. As the temperature increased, the $T_{1\rho}$ values increased at all temperatures. The ^{13}C $T_{1\rho}$ values for CH_2-b close to NH_3 are smaller than those for CH_2-a; this indicates that the ^{13}C $T_{1\rho}$ values for CH_2-b are more

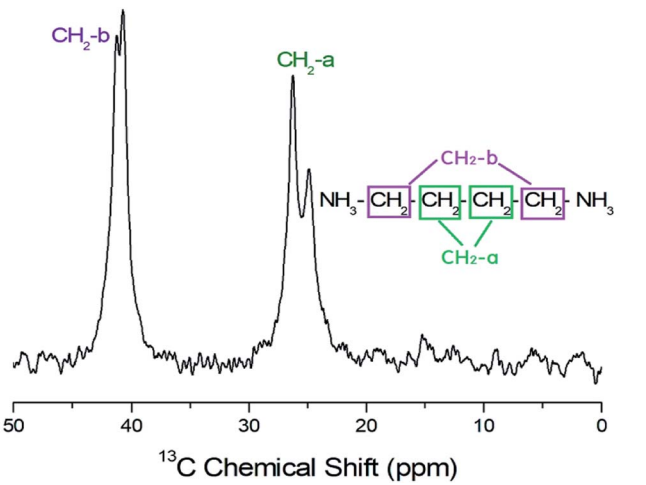

Fig. 7 MAS ^{13}C NMR chemical shifts for CH_2-a and CH_2-b of $[NH_3(CH_2)_4NH_3]ZnCl_4$ at 300 K.

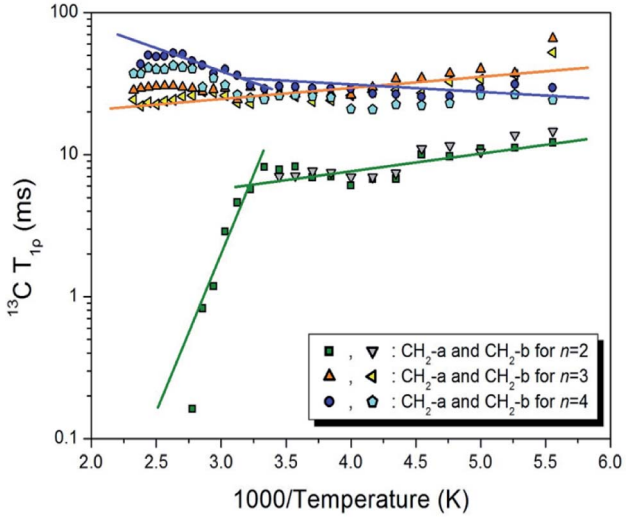

Fig. 8 ^{13}C NMR spin–lattice relaxation times $T_{1\rho}$ of $[NH_3(CH_2)_nNH_3]ZnCl_4$ (n = 2, 3, and 4) as a function of inverse temperature. The solid lines represent activation energy.

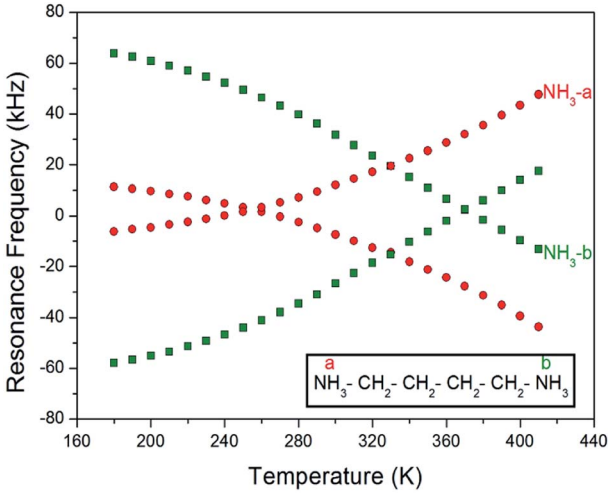

Fig. 9 ^{14}N resonance frequency of $[NH_3(CH_2)_4NH_3]ZnCl_4$ single crystal as a function of temperature.

flexible than those for CH_2-a. The E_a values represented by the solid lines at low and high temperatures are 0.72 ± 0.29 and 6.11 ± 0.58 kJ mol^{-1}, respectively.

To understand the effect of the length n of the CH_2 group in the $[NH_3(CH_2)_nNH_3]$ cation, we compared $[NH_3(CH_2)_2NH_3]ZnCl_4$, $[NH_3(CH_2)_3NH_3]ZnCl_4$, and $[NH_3(CH_2)_4NH_3]ZnCl_4$ with n = 2, 3, and 4. The ^{13}C $T_{1\rho}$ results are also shown in Fig. 8 for the three compounds (n = 2, 3, and 4) as a function of the inverse temperature. In the case of n = 2, the ^{13}C $T_{1\rho}$ value decreases sharply above 300 K with increasing temperature. The ^{13}C $T_{1\rho}$ value at 300 K is 8.35 ms, and at 430 K, it sharply drops to 0.16 ms.[28] The activation energies calculated from the slopes of the log $T_{1\rho}$ *vs.* inverse temperature curves are determined to be 2.23 ± 0.45 and 38.88 ± 7.33 kJ mol^{-1} below and above 300 K, respectively. In addition, the E_a values for CH_2-b below 300 K are almost identical to those of CH_2-a within the experimental error range. In the case of n = 3, the ^{13}C $T_{1\rho}$ values decreased slightly with increasing temperature but remained between 20 and 60 ms. E_a was 1.57 ± 0.21 kJ mol^{-1} at all temperatures.

3.5 Static ^{14}N NMR

Static ^{14}N NMR investigations of $[NH_3(CH_2)_4NH_3]ZnCl_4$ single crystals were conducted over a temperature range of 180–430 K. The ^{14}N spectra were obtained using the one-pulse method using static NMR. Two ^{14}N NMR signals were expected from the quadrupole interactions under a spin number of I = 1.[30] The ^{14}N NMR spectrum varied with increasing temperature, as shown in Fig. 9. The measurements were performed by keeping the c-axis of the single crystals parallel to the direction of the magnetic field. It was not easy to get ^{14}N were signals because we were measuring at the low frequency of 28.90 MHz. The four plots in the graph, shown in Fig. 9, were attributed to the two inequivalent NH_3-a and NH_3-b ions. The two inequivalent ^{14}N resonance lines due to NH_3-a and NH_3-b are related to the two types of ^{13}C resonance lines due to CH_2-a and CH_2-b. NH_3-a and NH_3-b were arbitrarily determined for NH_3. The four resonance lines of the two pairs decreased with increasing temperature to minima near 250 K (red circle) and 370 K (olive square), respectively, and then increased again. Symbols with the same colors indicate the same pairs for ^{14}N. In addition, the change in the ^{14}N resonance frequency with temperature is due to structural geometry change, which means a change in the quadrupole coupling constant.[34] the chemical shifts of the ^{14}N signals changed almost continuously without any anomalous changes. The changes in the ^{14}N chemical shift as a function of temperature were attributed to the variations in the structure of the N–H···Cl hydrogen bonds, indicating changes in the atomic configurations near the ^{14}N nuclei.

4. Conclusions

Based on information obtained from NMR analyses of the methylene chain length, the structural dynamics of the $[NH_3(CH_2)_nNH_3]$ cation in $[NH_3(CH_2)_nNH_3]ZnCl_4$ crystals were analyzed in this study. We compared the physical properties of previously reported $[NH_3(CH_2)_2NH_3]ZnCl_4$ and $[NH_3(CH_2)_3NH_3]ZnCl_4$ crystals with those of $[NH_3(CH_2)_4NH_3]ZnCl_4$ examined in this study.

The ^{1}H chemical shifts for the $NH_3(CH_2)_nNH_3$ cation (n = 2, 3, and 4) were found to be nearly temperature-independent. The two inequivalent CH_2-a and CH_2-b were distinguished through ^{13}C NMR experiments, and the two inequivalent ^{14}N were distinguished based on ^{14}N NMR results.

The behavior of $T_{1\rho}$ for molecular motions with a correlation time τ_C is described in two regimes: fast- and slow-motion regimes. At low temperatures, the ^{1}H $T_{1\rho}$ values for all three crystals indicated fast motion: $\omega_1\tau_C \ll 1$, $T_{1\rho}{}^{-1} \propto \exp(E_a/k_BT)$. Their values at high temperatures indicated slow motion: $\omega_1\tau_C \gg 1$, $T_{1\rho}{}^{-1} \propto \omega_1{}^{-2} \exp(E_a/k_BT)$.[30,33] However, the ^{13}C $T_{1\rho}$ values at low and high temperatures for n = 2 and 3 indicated slow

motion. In the case of $n = 4$, ^{13}C $T_{1\rho}$ at all temperatures undergoes the fast motion, unlike in the cases of $n = 2$ and 3. In addition, the ^{1}H and ^{13}C E_a values, measured according to the length of the CH_2 groups in the cation chain, decreased because ^{1}H and ^{13}C became more flexible with increasing length. According to the NMR $T_{1\rho}$ result, as the length of the cation increases, the motion of the methylene chain becomes flexible at high temperatures. This result correlates with the effect of electron–phonon interactions on the luminescence of single crystals of 2D perovskite reported by Gong *et al.*[35] The NMR measurements of $T_{1\rho}$, density functional theory simulations and experimental atomic displacements reveal that molecular motion was slowest and most rigid in the brightest emitter.

Solid-state NMR provides information of the material's thermal stability, structural change, and dynamics of the molecular motion depending on the temperature. The molecular motion differed according to the length of the cation and the temperature, and our solid-state NMR study on perovskites can therefore highlight potentials for each perovskite material for specific applications.

Conflicts of interest

There are no conflicts to declare.

Acknowledgements

This research was supported by the Basic Science Research program through the National Research Foundation of Korea, funded by the Ministry of Education, Science, and Technology (grant numbers 2018R1D1A1B07041593 and 2016R1A6A1A03012069).

References

1 A. R. Lim, *J. Solid State Chem.*, 2021, **295**, 121909.
2 N. Narita and I. Yamada, *J. Phys. Soc. Jpn.*, 1996, **65**, 4054.
3 D. B. Mitzi, *J. Chem. Soc., Dalton Trans.*, 2001, **1**, 1.
4 K. Pradeesh, J. J. Baumberg and G. Vijaya Prakash, *Appl. Phys. Lett.*, 2009, **95**, 173305.
5 Z. Cheng and J. Lin, *CrystEngComm*, 2010, **12**, 2646.
6 K. Pradeesh, G. S. Yadav, M. Singh and G. Vijaya Prakash, *Mater. Chem. Phys.*, 2010, **124**, 44.
7 S. Saikumar, J. J. Ahmad, G. Baumberg and G. Vijaya Prakash, *Scr. Mater.*, 2012, **67**, 834.
8 A. R. Lim, *J. Solid State Chem.*, 2021, **302**, 122438.
9 S. Ahmad, C. Hanmandlu, P. K. Kanaujia and G. Vijaya Prakash, *Opt. Mater. Express*, 2014, **4**, 1313.
10 S. Gonzalez-Carrero, R. E. Galian and J. Perez-Prieto, *Part. Part. Syst. Charact.*, 2015, **32**, 709.
11 B. Staskiewicz, O. Czupinski and Z. Czapla, *J. Mol. Struct.*, 2014, **1074**, 723.
12 B. Staskieqicz, I. Turowska-Tyrk, J. Baran, C. Gorecki and Z. Czapla, *J. Phys. Chem. Solids*, 2014, **75**, 1305.
13 Z. Czapla, J. Przeslawski, M. Crofton, J. Janczak, O. Czupinski, A. Ingram and M. Kostrzewa, *Phase Transitions*, 2017, **90**, 637.
14 S. K. Abdel-Adal, G. Kocher-Oberlehner, A. Ionov and R. N. Mozhchil, *Appl. Phys. A: Mater. Sci. Process.*, 2017, **123**, 531.
15 R. Kind, S. Plesko, P. Gunter, J. Ross and J. Fousek, *J. Phys. Chem. Solid.*, 2015, **75**, 1305.
16 M. F. Mostafa, A. S. Atallah and R. Emrick, *Appl. Phys.*, 1997, **81**, 4134.
17 C. Sourisseau, G. Lucazeau and A. J. Dianoux, *J. Phys.*, 1983, **44**, 967.
18 K. Chhor, J. F. Bocquet and C. Pommier, *J. Chem. Thermodyn.*, 1985, **17**, 379.
19 V. V. Eremenko, V. I. Fomin and V. S. Kurnosov, *Phys. B*, 1994, **194–196**, 187.
20 J.-C. Bissey, N. Filloleau, N.-B. Chanh, R. Berger and S. Flandrois, *Solid State Commun.*, 1998, **106**, 385.
21 M. M. Bogdan, M. I. Kobets and E. N. Khats'ko, *Low Temp. Phys.*, 1999, **25**, 192.
22 S. J. Lee, M. Y. Choi and A. R. Lim, *ACS Omega*, 2021, **6**, 15392.
23 W. T. A. Harrison, *Acta Crystallogr., Sect. E: Struct. Rep. Online*, 2005, **61**, m1951.
24 A. Kallel, J. Fail, H. Fuess and A. Daoud, *Acta Crystallogr., Sect. B: Struct. Crystallogr. Cryst. Chem.*, 1980, **36**, 2788.
25 W.-J. Yin, T. Shi and Y. Yan, *Adv. Mater.*, 2014, **26**, 4653.
26 W.-Q. Liao, Y. Zhang, C.-L. Hu, J.-G. Mao, H.-Y. Ye, P.-F. Li, S. D. Huang and R.-G. Xiong, *Nat. Commun.*, 2015, **6**, 7338.
27 B. Staskieqicz and A. Staskieqicz, *J. Phys. Chem. Solids*, 2017, **106**, 65.
28 A. R. Lim, *ACS Omega*, 2020, **5**, 31417.
29 A. R. Lim, S. H. Kim and Y. L. Joo, *Sci. Rep.*, 2021, **11**, 8408.
30 A. Abragam, *The Principles of Nuclear Magnetism*, Oxford University press, 1961.
31 R. K. Harris, *Nuclear Magnetic Resonance Spectroscopy*, Pitman, London, 1983.
32 N. Bloembergen, E. M. Purcell and R. V. Pound, *Phys. Rev.*, 1948, **73**, 679.
33 A. R. Lim, *RSC Adv.*, 2021, **11**, 17622.
34 M. B. Yoon, W. J. Lee and A. R. Lim, *RSC Adv.*, 2020, **10**, 34800.
35 X. Gong, O. Voznyy, A. Jain, W. Liu, R. Sabatini, Z. Piontkowski, G. Walters, G. Bappi, S. Nokhrin, O. Bushuyev, M. Yuan, R. Comin, D. McCamant, S. O. Kelley and E. H. Sargent, *Nat. Mater.*, 2018, **17**, 550.